InAs/InP Quantum Dash Semiconductor Coherent Comb Lasers and their Applications in Optical Networks

Zhenguo Lu, Jiaren Liu, Philip J. Poole, Youxin Mao, John Weber, Guocheng Liu, and Pedro Barrios

(Invited Paper)

***Abstract*—We report on the design, growth, and fabrication of InAs/InP quantum dash (QD) gain materials and their use in lasers for optical network applications. A noise performance comparison between QD and quantum well (QW) Fabry–Perot (F-P) lasers has been made. By using the QD gain material we have successfully developed and assembled C-band coherent comb laser (CCL) modules with an electrical fast feedback loop control system to ensure a targeted mode frequency spacing. The frequency spacing was maintained within $\pm$100 ppm and the operation wavelengths locked on the desired ITU grid within 0.01 nm over a period of several months. We also investigated a 25-GHz C-band QD CCL with an external cavity self-injection feedback locking (SIFL) system to reduce the optical linewidth of each individual channel to below 200 kHz in the wavelength range from 1537.55 nm to 1545.14 nm. The RF mode beating signal 3-dB bandwidth was also reduced from 9 kHz to approximately 500 Hz with this SIFL system. These QD CCLs with ultra-low relative intensity noise (RIN), ultra-narrow optical linewidth, and ultra-low timing jitter are excellent laser sources for multi-terabit optical networks. Using a 34.2 GHz QD CCL we demonstrate 10.8 Tbit/s (16QAM 48 $\times$ 28 GBaud PDM) coherent data transmission over 100 km of standard single mode fiber (SSMF) and 5.4 Tbit/s (PAM-4 48 $\times$ 28 GBaud PDM) aggregate data transmission capacity over 25 km of SSMF with error-free operation.**

***Index Terms*—Coherent comb lasers, coherent terabit/s networking systems, data center networks, integrated optics devices, optical communications, phase noise, quantum dash, quantum dot semiconductor mode-locked lasers, relative intensity noises, timing jitter.**

I. Introduction

As worldwide data traffic continues to grow, it becomes urgent to utilize communication resources optimally, facilitating capacity growth at reduced energy consumption. The enormous growth of internet data traffic imposes new challenges on the telecommunication industry, requiring the development of new advanced photonics components for next generation optical networks [1]. The waveguide-based coherent comb lasers (CCLs) with their ability to emit stable optical pulse trains at high repetition rate and narrow pulse widths are a promising technology for optical telecommunications [2]. Recently, there has been significant interest in optical CCLs and their benefits as monolithic sources of multiple wavelength channels for wavelength division multiplexing (WDM), dense-WDM (DWDM), super-channel, and coherent fiber communication systems with net data rates exceeding Terabit/s and high spectral efficiency [3]–[6]. Such CCLs can reduce costs and packaging complexity by replacing many separate lasers for each channel by a single laser chip [7]–[14].

Semiconductor mode-locked lasers (MLLs), which are perfect monolithic CCL sources, have many photonic applications for optical communications due to their compactness, mechanical stability and robustness, high potential repetition rates and low potential jitter, are very suitable for high-speed data transmission and switching, clock signal generation and electro-optic sampling [15]. As a result, monolithic MLLs have been extensively studied in bulk and quantum well (QW) semiconductor material systems for over 30 years [16]. It has been demonstrated for many years that replacing bulk layers or QWs with quantum dots or dashes (QDs) as the active gain medium for semiconductor lasers has resulted in a number of enhancements in laser device performance, such as reduced threshold current density or increased material gain [17], lower sensitivity of the threshold current to temperature (T_0) [18], reduced chirp [19], lower threshold current density [20], high differential gain and small linewidth enhancement factor [21], [22], much broad spectral gain bandwidths [23] and much faster carrier dynamics [24]. In recent years we have developed InAs/InP QD MLLs i.e., QD CCLs with repetition rates from 10 GHz to 1000 GHz and a total output power up to 50 mW per facet at room temperature [25]–[31]. For these QD CCLs we have investigated noise performance, such as relative intensity noise (RIN) and phase noise of filtered individual wavelength channels, the RF beating signal of the whole coherent comb and timing jitter. These QD-based monolithic CCLs are very attractive laser sources with huge potential for use in multi-terabit/s networking systems

Manuscript received October 16, 2020; revised November 27, 2020; accepted December 2, 2020. Date of publication December 8, 2020; date of current version June 16, 2021. This work was supported by the National Research Council Canada's High Throughput and Secure Networks (HTSN) Program. *(Correponding author: Zhenguo Lu.)*

The authors are with the Advanced Electronics and Photonics Research Centre, National Research Council Canada, Ottawa, ON K1A 0R6, Canada (e-mail: zhenguo.lu@nrc-cnrc.gc.ca; jiaren.liu@nrc-cnrc.gc.ca; philip.poole@nrc-cnrc.gc.ca; youxin.mao@nrc-cnrc.gc.ca; john.weber@nrc-cnrc.gc.ca; guocheng.liu@nrc-cnrc.gc.ca; pedro.barrios@nrc-cnrc.gc.ca).

Color versions of one or more figures in this article are available at https://doi.org/10.1109/JLT.2020.3043284.

Digital Object Identifier 10.1109/JLT.2020.3043284

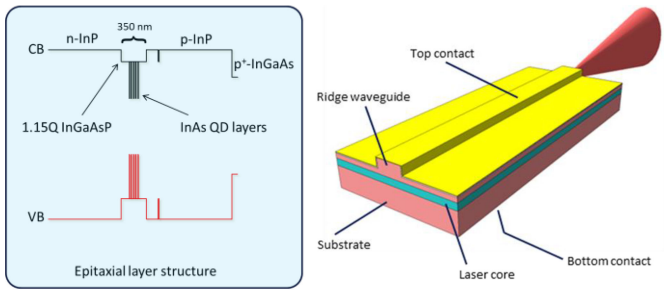

Fig. 1. (a) Band diagram for the laser structure of InAs/InP QD gain material and (b) schematics of a single lateral mode Fabry–Perot laser.

due to their compactness, ultra-low noise, large mode spacing, low electricity power consumption, simple fabrication, and their ability for hybrid integration with silicon substrates.

In this paper we report on the design, growth, and fabrication of InAs/InP QD Fabry-Perot (F-P) lasers and provide a comparison with QW based lasers with otherwise identical designs and layer structures. The QD lasers are then incorporated into modules with an electronic fast feedback system to lock their emitted wavelength combs onto the desired ITU grid, and with optical self-injection locking system to reduce optical linewidth. The suitability of these devices for use in high-speed optical networks is then demonstrated by measuring their performance using both PAM-4 and 16QAM data modulation formats.

II. Designs and Growth of QD Lasers

The lasers studied in this paper were grown on 3" n-type (100) InP substrates using chemical beam epitaxy (CBE). A typical laser structure design is shown schematically in Fig. 1(a). Fig. 1(b) shows a schematic of the finished single lateral mode F-P laser. The structure consisted of an n-type InP cladding, a 350 nm lattice matched 1.15 μm bandgap InGaAsP (1.15Q) core containing either the QWs or QDs, a p-type InP cladding (including an etch stop layer) and p+ InGaAs contact layer. The QW core consisted of four 60 Å thick 1.22% compressively strained QWs and 100Å 1.15Q barriers with room temperature photoluminescence (PL) emission at 1.539 μm. The QD core consisted of five layers of InAs quantum dashes with a period of 108 Å, also using 1.15Q barrier material. This structure provides both carrier and optical confinement in the QW/QD region. A double cap process was used for the QDs to precisely control the emission wavelength, resulting in room temperature PL at 1.555 μm. Fig. 2(a) shows a schematic cross-sectional diagram of an etched ridge-waveguide InAs/InP QD CCL. Fig. 2(b) shows a cross-sectional scanning electron microscopy (SEM) image of a five-layer InAs/InP QD core region. More detailed information of the QD CCL material growth is contained in [Ref. [32].

The laser wafers were fabricated into single lateral mode ridge waveguide lasers with a ridge width of 2.0 μm and were cleaved to form F-P laser cavities. Fig. 2(c) shows a cross-sectional SEM image of the facet of a fabricated F-P laser.

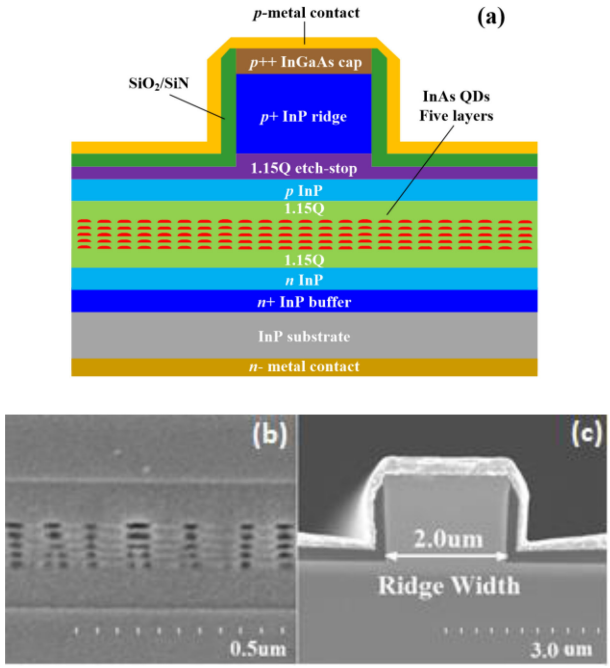

Fig. 2. (a) Schematic cross-sectional diagram of a shallow-etched ridge-waveguide InAs/InP QD CCL; (b) a cross sectional SEM image of the five-layer InAs/InP QD core region; (c) a cross-sectional SEM image showing the facet of a fabricated Fabry – Perot InAs/InP QD CCL.

Both facets were left uncoated. The lasers were driven with a low-noise laser diode driver, and tested on a temperature controlled heat sink maintained at 18 °C. The performance of the lasers was characterized using an Optical Spectrum Analyzer (OSA) (Anritsu MS9740A), Agilent N4371A Relative Intensity Noise Measurement Systems, a 50 GHz PXA Signal Analyzer (Keysight N9030A), a Finisar Ultra-Fast 100 GHz Photodetector XPDV4120R, an Optical Autocorrelator (Femtochrome Research Inc. FR-103HS), a Delayed Self-Heterodyne Interferometer (Advantest Q7332 & R3361A), an OE4000 Automated Laser Linewidth Measurement System (OEWaves Inc.), Santec Optical Tunable Filter OTF-350, Arbitrary Waveform Generator (Keysight M8195A), built-in 65 GHz Optical Detector (Keysight 86116C), Keysight Optical Modulation Analyzer N4392A, 86100D Infiniium DCA-X Wide-Bandwidth Oscilloscope, Intensity Modulator (Thorlab LN05-40-S-A-A-NS), SHF 46215B DP-QAM Transmitter with 10001B small main frame, RF Amplifier and Bias Controller (Anritsu AH34152A), Erbium-Doped Fiber Amplifiers (EDFAs) and other photonic components.

III. Performance of QD and QW F-P Lasers

In order to understand and illustrate the differences between QD and QW gain materials for CCL sources, we have designed, grown, and fabricated both QD and QW ridge waveguide F-P lasers with almost identical designs. These were grown in the same growth system and processed at the same time. They were fabricated into single-lateral mode ridge waveguide F-P lasers with a ridge width of 2 μm and a cavity length of approximately

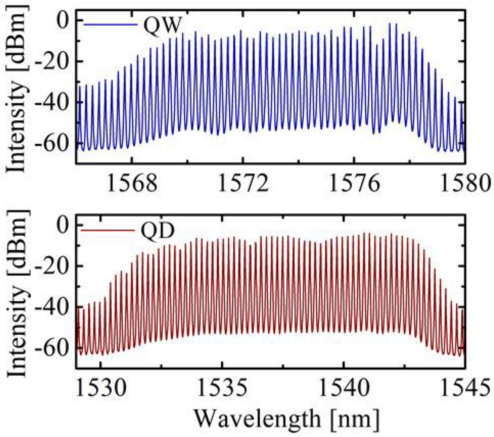

Fig. 3. Optical spectrum of the QW (upper curve) and QD (lower curve) lasers with an active length of 1500 μm at 300 mA and 18 °C.

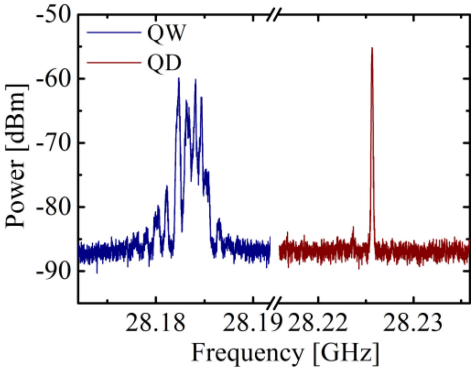

Fig. 4. The RF beating signals of both the QW laser (blue curve) and QD laser (red curve) with an active length of 1500 μm at 300 mA and 18 °C.

1500 μm, the cleaved facets were left uncoated. Fig. 3 shows the optical spectra of both the QW and QD F-P lasers with an OSA resolution of 0.01 nm when the operation conditions are 300 mA and 18 °C. From Fig. 3 we can see that the optical spectral broadness and gain flatness of the QD F-P laser are better than that of the QW F-P laser. Focusing all comb lines of these QW or QD lasers onto a high speed photodetector allowed us to monitor the mode beating signal using an RF signal analyzer (Keysight N9030A PXA with RBW of 10 kHz and VBW of 1.0 KHz in the span of 20 MHz, respectively). The RF beating signal (blue curve) around 28.183 GHz for the QW laser was very broad and unstable as shown in Fig. 4. In comparison we observe a very stable and sharp RF beating signal (red curve) at 28.225 GHz with the 3-dB electrical linewidth of less than 10 kHz from our QD F-P laser, also shown in Fig. 4. Their RF beating signals have clearly indicated that the QD F-P laser is an excellent mode-locked semiconductor laser, which both phase and amplitude of different longitudinal modes within QD F-P cavity have strongly synchronized and correlated each other [26], [27], [29]. But here the QW F-P laser is not a good mode-locked laser.

We have also investigated the noise performance, i.e., RIN and phase noise or optical linewidth, of individual longitudinal modes (wavelength channels) filtered by our tunable filter from both the QW and QD F-P lasers. Fig. 5 gives the RIN spectrum

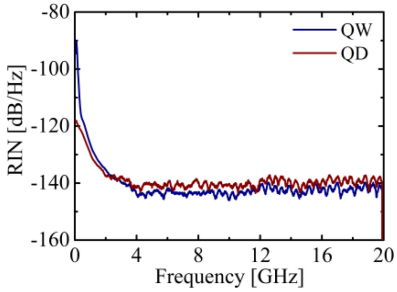

Fig. 5. The RIN spectrum of one filtered individual channel from both the QW F-P laser (red curve) and QD F-P laser (blue curve) with an active length of 1500 μm at 300 mA and 18 °C.

of one filtered individual channel from each of the QW and QD F-P lasers at 300 mA and 18 °C. Their integrated average RIN values in Fig. 5 are −113 dB/Hz for the QW laser with the wavelength of 1575 nm and −132.6 dB/Hz for the QD laser with the wavelength of 1542 nm in the frequency range from 10 MHz to 20 GHz. The difference in the integrated RIN is dominated by the low frequency noise, with the QD laser being at least 20 dB lower than the QW laser with otherwise identical designs. In Fig. 5, the individual longitudinal modes of both the QD and QW F-P lasers have shown much higher RIN values at very low frequencies of less than 1 GHz as compared with the RIN values of high frequencies of larger than 2 GHz. This is due to the high mode partition noise in strongly multimode semiconductor lasers [33] and the flicker noise or 1/f noise at the low frequency range.

Phase noise is another critical parameter for lasers used in high speed and coherent communication systems [34]. Here we have measured the optical linewidth of each filtered individual channel from both the QW and QD F-P lasers. The typical optical linewidths from the QD F-P laser are less than 3 MHz, but the optical linewidths from the QW F-P laser are very broad (>100 MHz). By using a tunable notch filter we have measured both RIN and phase noise spectra of all individual channels within the 6-dB optical bandwidth from both QW and QD F-P lasers at 300 mA and 18 °C. For the QD F-P laser the integrated average RIN values are less than −130 dB/Hz for all channels and the phase noise of each individual channel is between 0.9 MHz to 3 MHz. In comparison, the integrated average RIN values are larger than −113 dB/Hz and optical linewidth of all individual channels are bigger than 100 MHz for the QW F-P laser. The low RIN results indicate that filtered individual wavelength channels from the QD F-P laser are compatible with the requirements for data center Ethernet systems using data format PAM-4 at the data symbol rate of 28 GBaud [35]. These results clearly indicate that the QD F-P lasers are much better CCL sources compared to QW F-P lasers, and that the QD F-P lasers can be excellent monolithic CCL sources for multi-terabit/s networking systems.

IV. QD CCL Module Design and Performance

To demonstrate the practicality of the QD lasers in network systems, computer-controlled stabilized laser modules were

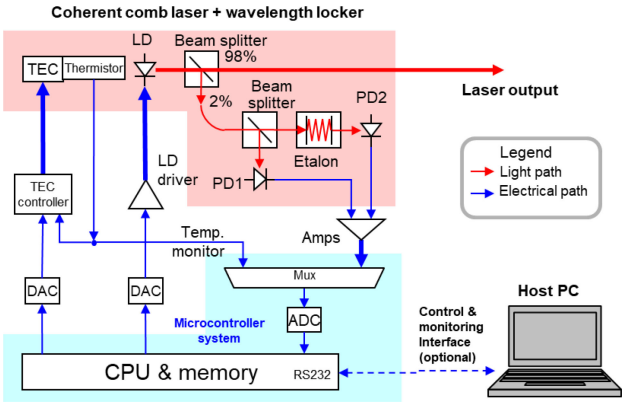

Fig. 6. Schematic of a QD CCL module and its electrical control system.

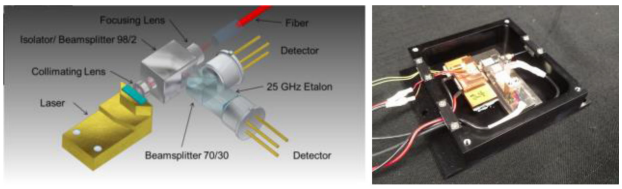

Fig. 7. (a) Schematics of the optical designs of a 25 GHz QD CCL and (b) an actual optical fiber pigtailed subassembly of the QD CCL block.

fabricated. The InAs/ InP QD CCL module design is shown schematically in Fig. 6. The laser was mounted on a thermoelectric cooler (TEC) for temperature control. Light output from this laser was sent through a collimating lens, a two-stage C-band optical isolator and beam splitter. After the beam splitter, one beam was focused into an optical single-mode (SM) fiber by another collimating lens. The second beam was sent through another beam splitter that directed part of the light to a reference photodiode (PD1), and the rest of the light through a high-finesse etalon to another photodiode (PD2). The etalon length and free spectral range (FSR) was designed to match the desired frequency grid spacing of the QD CCL. Fig. 7(a) shows the optical design schematic of the 25-GHz QD CCL. The total coupling loss from laser facet to SM fiber is approximately 2.4 dB. The rest of the system in Fig. 6 implements a two-input and two-output feedback loop which stabilizes the wavelength and output power. In addition, a user can use a single command to adjust the wavelength or power independently – without affecting the other. All optical components were actively aligned and assembled into a SM fiber pigtailed subassembly as shown in Fig. 7(b). The QD CCL block has dimensions of 60 × 60 × 32 mm, and was integrated into a 3U rack mountable case along with the power supply, microcontroller system and analog interface board. Fig. 8 shows a completed 3U rack mountable QD 25-GHz CCL module. In our uncontrolled laboratory environment we have continuously operated the laser module with the desired comb frequency of 25 GHz, with comb frequency spacing and absolute wavelength held to within ±100 ppm and ±0.01 nm, respectively, over a period of several months.

Fig. 8. A completed rack mount QD C-band 25 GHz CCL module.

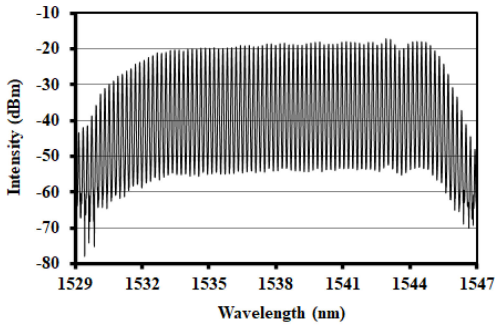

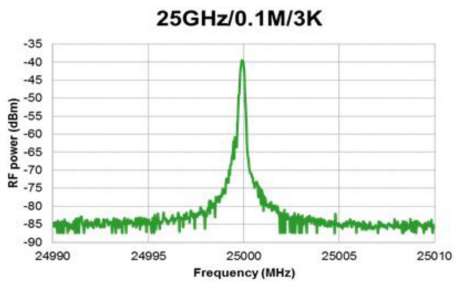

Fig. 9. (a) Optical spectrum of a 25 GHz QD CCL and (b) its RF beating frequency of 25 GHz between any two adjacent channels at 380 mA and 20 °C.

Fig. 9 (a) and (b) show the optical spectrum and its RF beat spectrum of an InAs/InP QD C-band CCL with the active length of 1693 μm giving a mode spacing of 25 GHz. The center wavelength is 1539.21 nm and the 6 dB optical bandwidth is 11.85 nm, providing over 60 channels with an optical signal-to-noise ratio (OSNR) of more than 40 dB. The RF beat signal was obtained by focusing all wavelength channels simultaneously onto a fast photodiode and feeding the signal to an RF signal analyzer. The RF beat signal of 25 GHz is obtained for a QD laser drive current of 380 mA and an operating temperature of 20 °C. From L-I-V curves a lasing threshold current of 48 mA, single facet slope efficiency of 0.13 mW/mA, and a series resistance of 1.46 Ohm were determined. The average output power was 42 mW per facet at 380 mA and 20 °C. A programmable optical filter was used to select single wavelength channels, and combinations of adjacent channels for measurement of inter-channel beat frequencies and channel noise. We clearly observe a RF beating frequency of 25 GHz with the RF linewidth of approximately 10 kHz as

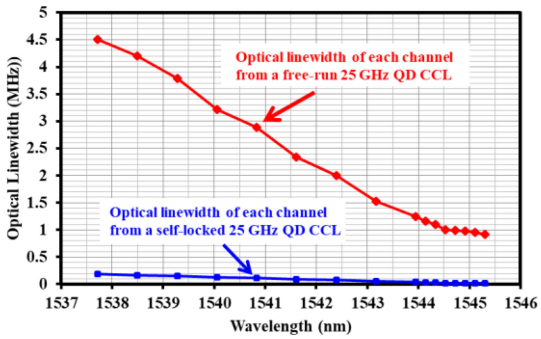

Fig. 10. Optical linewidth of a selection of individual filtered channels from the 25 GHz C-band QD CCL versus channel wavelength under the same operation conditions with (blue points) and without (red points) the self-injection feedback locking (SIFL) system.

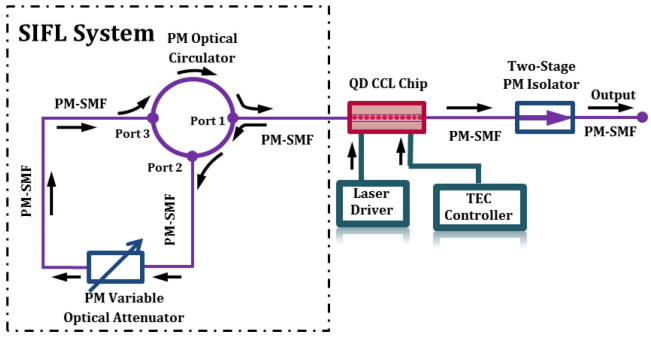

Fig. 11. A schematic of the ultra-narrow linewidth QD CCL using an external cavity self-injection feedback locking (SIFL) system. All components are polarization-maintaining.

shown in Fig. 9(b). Optical intensity autocorrelation pulse trains show pulses with an extinction ratio of larger than 25 dB with a 40 ps period, corresponding to the repetition rate of 25 GHz, and a pulse width of approximately 600 fs. These results clearly indicate that this QD laser is mode-locked where the different longitudinal modes have a well-defined phase relationship with each other [26], [27], [29] resulting in an excellent CCL source.

Fig. 10 shows, for an unpackaged 25-GHz QD CCL device, the measured optical linewidths calculated from the frequency noise spectra (red points) for a representative grouping of filtered wavelength channels from the laser versus channel wavelength over 39 channels. The laser output from the front facet of the QD CCL is coupled to an anti-reflection (AR) coated lensed polarization-maintaining (PM) SM fiber. A two-stage PM optical isolator is used to prevent any reflection back to the laser cavity from the measurement system. All measurements of the laser are characterized using this fiber output from the front facet. The optical linewidth of each individual channel is between 920 kHz and 4.51 MHz, which is at the limit of being good enough for use as a laser source for tens Tbit/s and beyond coherent optical networking systems. The decrease in linewidth when going to longer wavelength is typical of the behaviour observed for all of our QD F-P lasers [36], [37]. The possible reasons have been explained in reference paper [31].

In order to narrow the optical linewidth of all individual wavelength channels of the laser simultaneously, we have developed an external cavity self-injection feedback locking (SIFL) system [38], [39], shown schematically in Fig. 11. The external SIFL system is coupled to the back-facet of the laser using an AR-coated lensed PM SM fiber which is connected to port 1 of a PM optical circulator (OC). The output from port 2 of the PM OC passes through a PM variable optical attenuator (VOA), and back into port 3 of the PM OC. The circulating light is then reinserted at the back-facet of the laser cavity through port 1 of the PM OC and the AR coated lensed PM SM fiber. The physical length of this external cavity SIFL system is approximately 8 m. The above design provides an external cavity that is weakly coupled to the QD laser, where the degree of feedback is controlled using the PM VOA. The stable locking regime of the feedback laser power, which is coupled back from the SIFL system, is from 5×10^{-4} to 5×10^{-5} of the laser output power from the rear facet in Fig. 11. We have increased the external cavity length by many meters and can obtain equivalent linewidth narrowing by adjusting both the VOA and laser drive current. Thus, while the external cavity length is an important parameter, the linewidth narrowing is not critically sensitive to the cavity length.

Using this SIFL system at the rear-facet of the laser we observed a reduction of the optical linewidth of all laser lines by more than an order of magnitude, as shown in Fig. 10 (blue circle points). Optimization of the feedback strength by tuning the VOA resulted in linewidth values of each individual channel being simultaneously reduced to between 12 kHz and 198 kHz over the 39 channels. All channels from 1537.55 nm to 1545.14 nm originally had optical linewidths from 920 kHz to 4.51 MHz and are now less than 200 kHz, varying from 1.3% to 4.4% of the original linewidth. Even though the linewidths are dramatically reduced we observe no changes in the RIN values of each individual channel with and without the external SIFL system.

Typical average-integrated RIN values of the individual channels from this QD CCL are approximately - 130 dB/Hz in the frequency range from 10 MHz to 20 GHz. Unlike feedback schemes where just one wavelength is injected into the laser [40], we observed no changes in the shape of overall lasing spectrum. Fig. 12 shows the normalized RF beating signal spectra between two adjacent laser lines with and without the external cavity SIFL system. A substantial reduction in 3 dB linewidth from 9 kHz to 500 Hz with feedback, and a corresponding drop in baseline level (-27 dB to -50 dB) is observed. The timing jitter of the QD CCL with the SIFL system has been significantly decreased [41]. Recently by using an external-cavity optical feedback to reduce the optical phase noises of each individual channel, 32QAM WDM transmission at 12 Tbit/s using a quantum-dash mode-locked laser diode has been demonstrated in the reference [42].

V. Multi-Terabit Data Transmissions by a QD CCL

In order to verify that the QD CCLs are good enough for multi-terabit/s network applications we have used the 34.2 GHz C-band QD CCL to run PAM-4 and 16-QAM data format signals

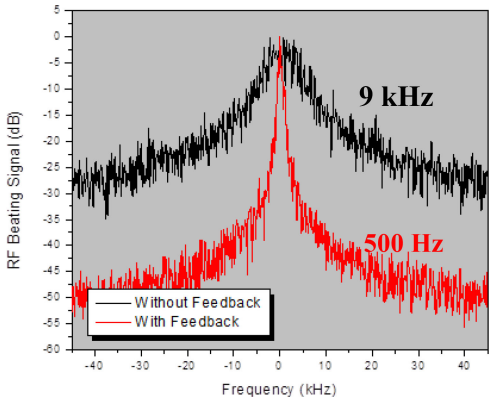

Fig. 12. Normalized RF beating signals of a 25 GHz QD CCL in the same operation conditions with (red curve) and without (black curve) the self-injection feedback locking (SIFL) system.

back-to-back (B2B) and over a long distance SSMF. Fig. 13(a) shows the optical spectrum of a QD CCL with an active length of 1227 μm, which gives a frequency spacing of 34.2 GHz at 350 mA and 18 °C with a single facet output power of 40 mW. The center wavelength is 1554.22 nm and the 6 dB bandwidth is 12.96 nm, providing 48 channels with the OSNR of more than 40 dB. Our measured L-I-V curves give that the lasing threshold current is 46 mA with the slope efficiency of 0.133 mW/mA and a series resistance of 1.52 Ohm. The RF beating signal is presented in Fig. 13(b) showing a sharp fundamental RF beating frequency at 34.224 GHz and a SNR of larger than 45 dB. The inset shows the RF linewidth with a Lorentzian fit. The 3 dB linewidth is 1.688 kHz, and such an extremely narrow linewidth leads to ultra-low pulse-to-pulse time jitter value of 2.59 fs [41] and phase noise [43].

Fig. 14(a) shows the RIN spectra for both the whole lasing spectrum and three filtered channels of 1557.484 nm, 1548.932 nm and 1558.596 nm. We achieve an integrated average RIN value less than -160.5 dB/Hz for the whole laser, with the upper bound set by the instrument limited RIN measurement floor. For the three filtered channels the integrated average RIN value increases to about −130.5 dB/Hz. The low frequency RIN does not exceed −118 dB/Hz for our device unlike the measurements shown in [Ref. [44] which is up to −90 dB/Hz. The integrated RIN values for all 48 filtered individual channels are approximately −130 dB/Hz in the frequency range from 10 MHz to 10 GHz. Fig. 14(b) shows the optical linewidth of each of the filtered individual channels from 1547.855 nm to 1560.812 nm at 350 mA and 18 °C. The average optical linewidth of each mode is around 1.5 MHz. The left inset is a comparison of the frequency noise spectra from three filtered wavelength channels at 1551.824 nm, 1552.924 nm and 1553.474 nm. The right inset is the single-sideband (SSB) phase noise measurement of the RF beating signal in the range from 100 Hz to 1 MHz. A strongly suppressed phase noise is observed over the entire frequency range of the carrier offset. The good noise performance is believed to benefit from the low amplified spontaneous emission (ASE) noise and low confinement factor properties of the QD CCL material [21], [22].

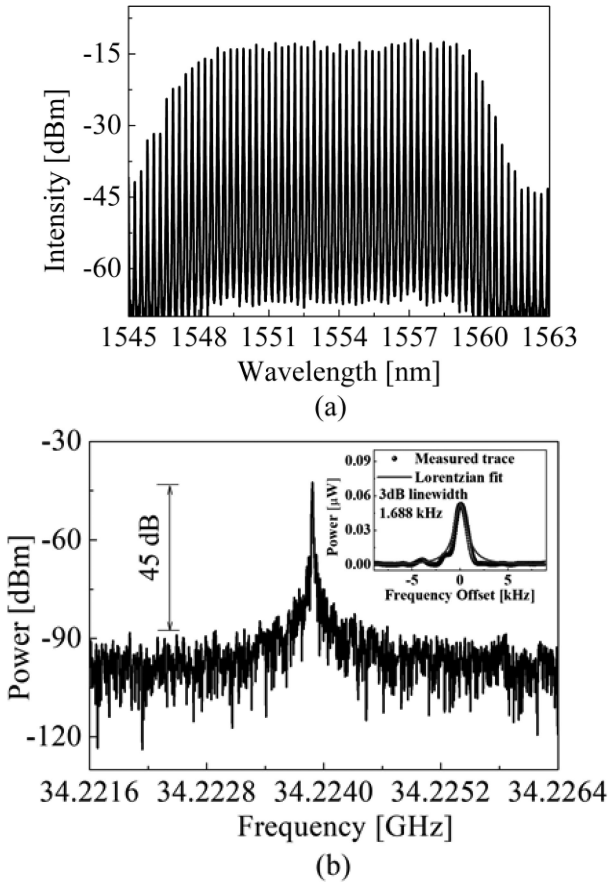

Fig. 13. (a) Optical spectrum of a QD-MLL with a cavity length of 1227 μm, measured at 350 mA and 18 °C (Noise floor: −60 dBm and resolution bandwidth (RBW): 0.01 nm); (b) RF beating frequency of 34.224 GHz between any two adjacent channels (RBW: 5 kHz). The inset is the narrow span RF peak with Lorentzian fit (RBW: 1 kHz).

Fig. 15 shows the experimental setup for the PAM-4 or 16-QAM data transmission. At the dual polarization (DP) I/Q optical modulator side (T_X), 28 GBaud PAM-4 or 16-QAM base-band signals are created by using an Arbitrary Waveform Generator generating a pseudo-random bit sequence (PRBS) with a pattern length of $2^{15}-1$ bits at a symbol rate of 28 Gbit/s non-return to zero (NRZ) on two uncorrelated channels (*IY/IX*). A root-raised-cosine (RRC) filter is applied with the roll-factor of 0.35 for Nyquist pulse filtering. Thermally stable nested lithium niobate ($LiNbO_3$) Mach-Zehnder modulators (MZMs) of the I/Q optical modulator are driven by the Arbitrary Waveform Generator for data modulation. At the receiver side (R_X), the modulated signal is first amplified by $EDFA_3$, and the optical bandpass filter $OBPF_2$ is used to filter out the ASE from the $EDFA_3$. The inset in Fig. 15 shows the optical spectra of one filtered channel at 1552.924 nm, at the output before MZMs and that after 16-QAM modulation.

The Keysight OMA coherently receives the signals using a free-running local oscillator (LO). Combined with the software package offered by the OMA, a matched RRC filter is executed to mitigate the effects of white noise and clock recovery is carried out to compensate for any sampling phase and frequency offset

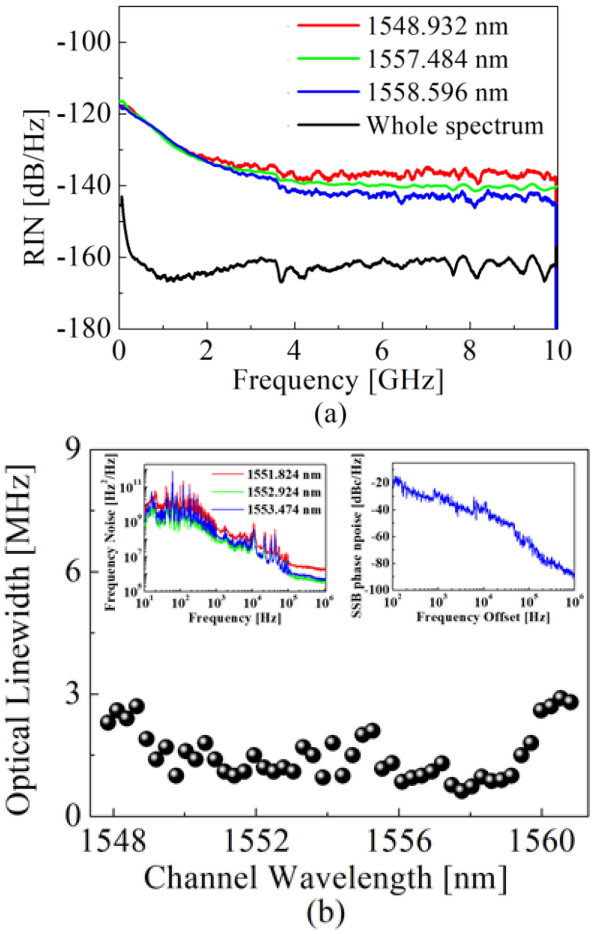

Fig. 14. (a) Measured RIN for the whole laser and three filtered channels in the frequency range from 10 MHz to 10 GHz. (b) Optical linewidth of the filtered individual channels from 1547.855 nm to 1560.812 nm at 350 mA and 18 °C. The left inset is a comparison of the frequency noise spectra from three filtered channels of 1551.824 nm, 1552.924 nm and 1553.474 nm. The right inset is the single-sideband (SSB) phase noise of the RF beating signal.

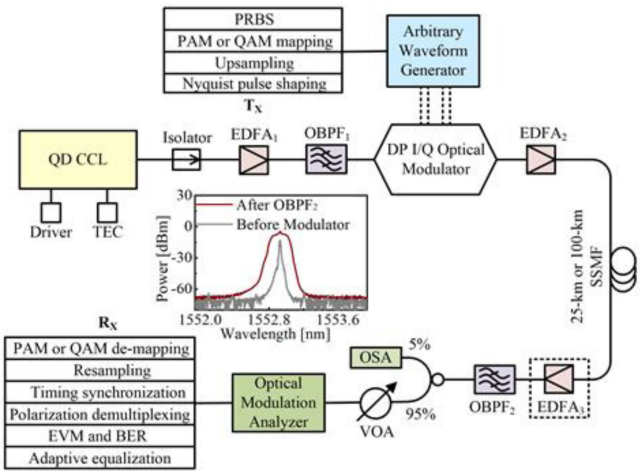

Fig. 15. Experimental setup of PAM-4 or 16-QAM data transmissions with the DP I/Q optical modulator (T_X) and the receiver (R_X). $EDFA_3$ is only used for 25 km or 100 km SSMF transmission. The inset shows the spectra of one filtered channel at 1552.924 nm, include after $OBPF_2$ and before OMA.

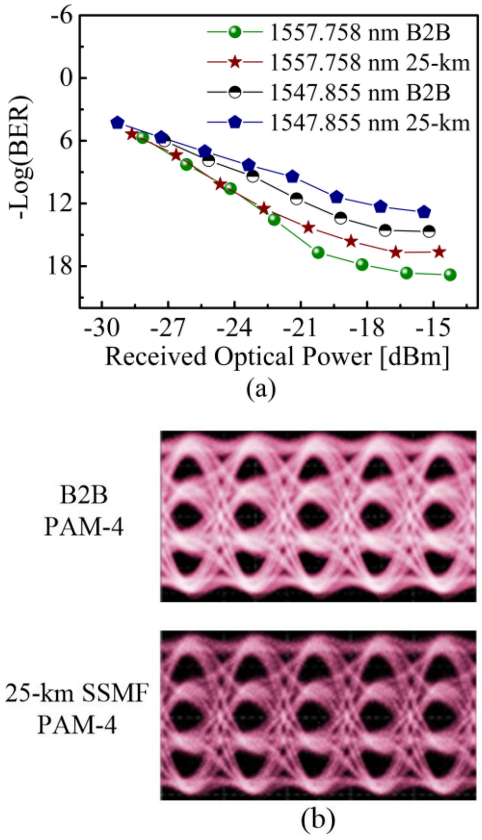

Fig. 16. (a) BER evaluation versus received optical power for B2B and after 25 km of SSMF transmission using the comb lines located at 1557.758 nm and 1547.855 nm; and (b) corresponding eye diagram for a selected channel at 1557.758 nm after B2B and 25 km of SSMF transmission.

that may exist between the transmitter and receiver clocks. The digitized signals undergo a number of digital signal processing (DSP) steps, including timing recovery, frequency offset compensation, carrier phase compensation, Kalman filtering, and adaptive equalization. Finally, the output PAM-4 or 16-QAM signals are decoded for error vector magnitude (EVM) measurement and BER evaluation. The BER performance is evaluated based on the EVM measurement. A VOA can be added before the OMA to control the received optical power. The inset shows the optical spectra of one filtered channel at 1552.924 nm, at the output before MZMs and after PAM-4 or 16-QAM modulation. The modulated optical signal is transmitted both for B2B configuration and over 25 km or 100 km SSMF, respectively.

We have measured the EVM and corresponding BER evaluation at the same received optical power of −15 dBm for all individual channels. The EVMs are from 7.8% to 13.5% and from 7.5% to 14.7%, respectively, after B2B and 25 km SSMF transmission (chromatic dispersion of 17 ps/nm/km). For some channels, the performance after 25 km SSMF transmission is better than that of B2B configuration due to the dispersion of the fiber cancelling the effect of the chirp induced by the optical modulator [45], [46]. Using a VOA before the OMA to control the received optical power, Fig. 16(a) shows the dependence of

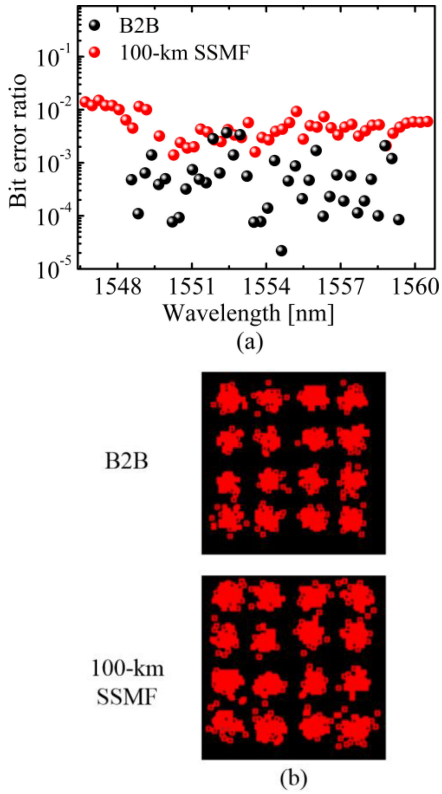

Fig. 17. (a) Measured BER versus wavelength and (b) observed constellation diagram for selected channel of 1552.92 nm for B2B and 100 km SSMF transmission.

BER evaluation on received optical power for the carriers located at 1557.758 nm and 1547.855 nm for B2B and after 25 km of SSMF transmission. The power penalty at the BER of 10^{-9} is free for the measured channel at 1557.758 nm and 1.5 dB for the channel at 1547.855 nm. The BER floors can be observed around −15 dBm. One of the comb lines chosen (1547.855 nm) is at the short wavelength edge, the other (1557.758 nm) closer to the center of the lasing spectrum. The short wavelength line has lower power, higher RIN, and larger optical linewidth, all of which likely contribute to the raised noise floor. Fig. 16(b) shows the measured eye diagram for the channel at 1557.758 nm after B2B and 25 km SSMF transmission. Open and clear eyes can be demonstrated and the aggregate data transmission capacity of 5.4 Tbit/s (PAM-4 48 × 28 GBaud PDM) is achieved by only using a single 34.2 GHz QD CCL.

Fig. 17(a) shows the transmission results using the 16-QAM data format at a symbol rate of 28 GBaud with a PRBS pattern length of $2^{15}-1$. All selected channels exhibit BERs performance below the 7% HD-FEC limit (BER = 4×10^{-3}) after B2B transmission and 20% SD-FEC limit (BER = 1.6×10^{-2}) after 100 km SSMF (chromatic dispersion of 17 ps/nm/km). Fig. 17(b) shows the measured constellation diagram for the channel at 1552.924 nm after B2B and 100 km SSMF transmission. The aggregate raw data transmission capacity of 10.8 Tbit/s (16-QAM 48 × 28 GBaud PDM) is demonstrated by using just a single 34.2 GHz C-band QD CCL.

VI. Conclusion

We have reported the design, growth and fabrication of the InAs/InP QD gain materials and the noise performance of the F-P cavity QD lasers as compared with that of a QW F-P cavity laser with the almost identical designs and layer structures. These lasers were grown in the same growth system and processed at the same time, in order to verify that the QD gain materials are better than the QW gain materials for CCL sources in terms of the noise performance of each individual channel. By using QD gain materials we have developed and assembled several ultra-low intensity noise and ultra-narrow optical linewidth QD CCL modules utilizing an electrical fast feedback loop control system to ensure the frequency spacing within the accuracy of less than ±100 ppm and to stabilize their operation wavelengths on the desirable ITU grid within 0.01 nm over an operation period of several months. We have demonstrated a 34.2 GHz C-band QD CCL which provides 48 individual channels with an OSNR of more than 40 dB. This QD CCL has shown ultra-low intensity and phase noise performance. The integrated RIN value for all 48 filtered individual channels are approximately −130 dB/Hz and the average optical linewidth is 1.5 MHz. By employing 48 wavelength channels as optical carriers, 5.4 Tbit/s PAM-4 aggregate data transmission capacity is demonstrated with the base modulation rate of 28 GBaud over 25 km SSMF. We have also used those 48 channels from this 34.2 GHz QD CCL as optical carriers, a system-level 10.8 Tbit/s 16-QAM signal detection is demonstrated with the transmission at 28 GBaud both for B2B and over 100 km SSMF configuration. The above achievements are a significant step towards a low-cost, chip-scale, high wavelength channel count laser source for large-scale optical networking systems with tens Tbit/s data transmission capabilities.

Acknowledgment

The authors thank their colleagues Dr. Siegfried Janz, Dr. Sylvain Raymond, Dr. Chun-Ying Song, Dr. Daniel Poitras, Dr. Shoude Chang, Mr. Martin Vachon, Dr. Shurui Wang, Mr. Craig Storey, Mrs. Ping Zhao and Dr. Heping Ding for their kind help toward research work.

References

[1] C. J. McKinstrie, N. Cheng, and X. Liu, "Enabling optical component technologies for next-generation broadband optical access," SPIE Photon. West 2018, San Francisco, CA, USA, Invited Paper 10561-7, Jan. 27 - Feb. 1, 2018.

[2] D. Arsenijevi´c, M. Kleinert, and D. Bimberg, "Breakthroughs in photonics 2013: Passive mode-locking of quantum-dot lasers," *IEEE Photon. J.*, vol. 6, no. 2, pp. 1–6, Aug. 2014.

[3] C. Weimann *et al.*, "Silicon-organic hybrid (SOH) frequency comb sources for terabit/s data transmission," *Opt. Express*, vol. 22, no. 3, pp. 3629–3639, Feb. 2014.

[4] V. Ataie *et al.*, "Flex-grid compatible ultrawide frequency comb source for 31.8 Tb/s coherent transmission of 1520 UDWDM channels," in *Proc. Proc. 2014 Opt. Fiber Commun. Conf.*, San Francisco, CA, USA, Postdeadline, Mar. 2014, Paper Th5B.7.

[5] Z. G. Lu, "Quantum-dot coherent comb lasers for terabit optical networking systems," in *Proc. SPIE, Integr. Opt.: Devices, Mater., Technol. XXIII*, San Francisco, CA, USA, Invited Paper 109210N, Mar. 2019.

[6] S. Liu *et al.*, "High-channel-count 20 GHz passively mode-locked quantum dot laser directly grown on si with 4.1 Tbit/s transmission capacity," *Optica*, vol. 6, no. 2, pp. 128–134, 2019.
[7] B. Corcoran *et al.*, "Ultra-dense optical data transmission over standard fibre with a single chip source," *Nat. Commun.*, vol. 11, no. 1, pp. 1–7, May 2020.
[8] Z. G. Lu, J. R. Liu, Y. X. Mao, C. Y. Song, J. Weber, and P. J. Poole, "12.032 Tbit/s coherent transmission using an ultra-narrow linewidth quantum dot 34.46-GHz C-band coherent comb laser," in *Proc. SPIE*, Feb. 2019, Art. no. 10947.
[9] H. Hu *et al.*, "Single-source chip-based frequency comb enabling extreme parallel data transmission," " *Nat. Photon.*, vol. 12, pp. 469–473, Aug. 2018.
[10] Z. G. Lu *et al.*, "2.24 Tbit/s PAM-4 transmission by an InAs/InP quantum dot mode-locked laser," in *Proc. SPIE Photon. West*, San Francisco, CA, USA, Feb. 2019, vol. 10946, Art. no. 109460A.
[11] P. Marin-Palomo *et al.*, "Comb-based WDM transmission at 10 Tbit/s using a DC-driven quantum-dash mode-locked laser diode," *Opt. Express*, vol. 27, no. 22, pp. 31110–31129, 2019.
[12] G. C. Liu *et al.*, "Passively mode-locked quantum dash laser with 5.4 Tbit/s PAM-4 transmission capacity," *Opt. Express*, vol. 28, no. 4, pp. 4587–4593, Feb. 2020.
[13] J. N. Kemal *et al.*, "Coherent WDM transmission using quantum-dash mode-locked laser diodes as multi-wavelength source and local oscillator," *Opt. Express*, vol. 27, no. 22, pp. 31164–31175, 2019.
[14] G. C. Liu *et al.*, "A passive mode-locked quantum dot laser with 10.8 Tbit/s transmission over 100-km SSMF," in *Proc. Opt. Fiber Commun.*, San Diego, CA, USA, Mar. 2020, Paper W2A.2.
[15] Q. Wada, "Femtosecond all-optical devices for ultrafast communication and signal processing," *New J. Phys.*, vol. 6, pp. 183–216, Nov. 2004.
[16] L. A. Jiang, E. P. Ippen, and H. Yokoyama, *Semiconductor Mode-Locked Lasers as Pulse Sources for High Bit Rate Data Transmission*. Berlin & Heidelberg: Springer, 2007, pp. 21–51.
[17] M. Asada, Y. Miyamoto, and Y. Suematsu, "Gain and the threshold of three-dimensional quantum-box lasers," *IEEE J. Quantum Electron.*, vol. QE-22, no. 9, pp. 1915–1921, Sep 1986.
[18] Y. Arakawa and H. Sakaki, "Multi-dimensional quantum well laser and temperature dependence of its threshold current," *Appl. Phys. Lett.*, vol. 40, pp. 939–941, 1982.
[19] H. Saito, K. Nishi, A. Kamei, and S. Sugou, "Low chirp observed in directly modulated quantum dot lasers," *IEEE Photon. Technol. Lett.*, vol. 12, no. 10, pp. 1298–1300, Oct. 2000.
[20] D. G. Deppe, K. Shavritranuruk, G. Ozgur, H. Chen, and S. Freisem, "Quantum dot laser diode with low threshold and low internal loss," *Electron. Lett.*, vol. 45, no. 1, pp. 54–56, 2009.
[21] Z. J. Jiao *et al.*, "Linewidth enhancement factor of InAs/InP quantum dot lasers around 1.5 μm.", *Opt. Commun.*, vol. 285, nos. 21/22, pp. 4372–4375, Oct. 2012.
[22] T. C. Newell, D. J. Bossert, A. Stintz, B. Fuchs, K. J. Malloy, and L. F. Lester, "Gain and linewidth enhancement factor in inas quantum-dot laser diodes," *IEEE Photon. Technol. Lett.*, vol. 11, no. 12, pp. 1527–1529, Dec. 1999.
[23] Z. G. Lu *et al.*, "Ultra-broadband quantum-dot semiconductor optical amplifier and its applications," in *Proc. Opt. Fiber Commun. Conf.*, Anaheim, CA, USA, Mar. 2007, Paper JThA33.
[24] A. J. Zilkie *et al.*, "Carrier dynamics of quantum-dot, quantum-dash, and quantum-Well semiconductor optical amplifiers operating at 1.55 μm," *IEEE J. Quantum Electron.*, vol. 43, no. 11, pp. 982–991, Nov. 2007.
[25] J. R. Liu *et al.*, "Uniform 90-channel multiwavelength InAs/InGaAsP quantum dot laser," *Electron. Lett.*, vol. 43, no. 8, pp. 458–460, Apr. 2007.
[26] Z. G. Lu, J. R. Liu, S. Raymond, P. J. Poole, P. J. Barrios, and D. Poitras, "312-fs pulse generation from a passive C-band InAs/InP quantum dot mode-locked laser," *Opt. Express*, vol. 16, no. 14, pp. 10835–10840, Jul. 2008.
[27] Z. G. Lu *et al.*, "An L-band monolithic InAs/InP quantum dot mode-locked laser with femtosecond pulses," *Opt. Express*, vol. 17, no. 16, pp. 13609–13614, Aug. 2009.
[28] J. R. Liu, Z. G. Lu, S. Raymond, P. J. Poole, P. J. Barrios, and D. Poitras, "Dual-wavelength 92.5 GHz self-mode-locked InP-based quantum dot laser," *Opt. Lett.*, vol. 33, no. 15, pp. 1702–1704, Aug. 2008.
[29] Z. G. Lu *et al.*, "Ultra-high repetition rate InAs/InP quantum dot mode-locked lasers," *Opt. Commun.*, vol. 284, no. 9, pp. 2323–2326, May 2011.
[30] Z. J. Jiao *et al.*, "Tunable terahertz beat signal generation from an InAs/InP quantum-dot mode-locked laser combined with external-cavity," *IEEE Photon. Technol. Lett.*, vol. 24, no. 6, pp. 518–520, Mar. 2012.
[31] Z. G. Lu *et al.*, "High performance InAs/inP quantum dot 34.462-GHz C-band coherent comb laser module," *Opt. Express*, vol. 26, no. 2, pp. 2160–2167, Jan. 2018.
[32] P. J. Poole, K. Kaminska, P. Barrios, Z. G. Lu, and J. R. Liu, "Growth of inas/inp-based quantum dots for 1.55 μm laser applications," *J. Cryst. Growth*, vol. 311, no. 6, pp. 1482–1486, 2009.
[33] R. H. Wentworth, G. E. Bodeep, and T. E. Darcie, "Laser mode partition noise in lightwave systems using dispersive optical fiber," *J. Lightw. Technol.*, vol. 10, no. 1, pp. 84–89, Jan. 1992.
[34] P. Marin *et al.*, "8.32 Tbit/s coherent transmission using a quantum-dash mode-locked laser diode," in *Proc. Conf. Lasers Electro-Opt.*, San Jose, CA, USA, Jun. 2016, Paper STh1F.1.
[35] N. Eiselt *et al.*, "Real-time 200 Gb/s (4×56.25 Gb/s) PAM-4 transmission over 80 km SSMF using quantum-dot laser and silicon ring-modulator," in *Proc. Opt. Fiber Commun. Conf.*, Los Angeles, CA, USA, Mar. 2017, Paper W4D.
[36] Z. G. Lu *et al.*, "Integrated InAs/InP quantum dot coherent comb lasers," (Invited paper), in *Proc. SPIE Photon. West*, San Francisco, CA, USA, Jan./Feb., 2017, pp. 10107–10118.
[37] J. Cartledge and M. O'Sullivan, "Time- and frequency-domain characterization of the relative intensity noise of a quantum-dot frequency comb source laser," *IEEE J. Sel. Top. Quantum Electron.*, vol. 25, no. 6, Nov./Dec. 2019, Art. no. 1900809.
[38] Z. Lu, J. Liu, P. Poole, C. Y. Song, and S. D. Chang, "Stable linewidth narrowing of a coherent comb laser," US Patent 0036304A1, 2019.
[39] Z. G. Lu, J. R. Liu, P. J. Poole, C. Y. Song, and S. D. Chang, "Ultra-narrow linewidth quantum dot coherent comb lasers with self-injection feedback locking," *Opt. Express*, vol. 26, no. 9, pp. 11909–11914, Apr. 2018.
[40] E. Sooudi *et al.*, "Injection-locking properties of InAs/InP-based mode-locked quantum-dash lasers at 21 GHz," *IEEE Photon. Technol. Lett.*, vol. 23, no. 20, pp. 1544–1546, Oct. 2011.
[41] Y. Mao, J. Liu, Z. Lu, C. Song, and P. J. Poole, "Ultra-low timing jitter of quantum dash semiconductor comb lasers with self-injection feedback locking," *IEEE J. Sel. Topics. QE*, vol. 25, no. 6, Nov. 2019, Art. no. 1900607.
[42] J. N. Kemal *et al.*, "32QAM WDM transmission at 12 Tbit/s using a quantum-dash mode-locked laser diode (QD-MLLD) with external-cavity feedback," *Opt. Express*, vol. 28, no. 16, pp. 23594–23608, Aug. 2020.
[43] F. Lelarge *et al.*, "Recent advances on InAs/InP quantum dash based semiconductor lasers and optical amplifiers operating at 1.55 μm," *IEEE J. Sel. Top. Quantum Electron.*, vol. 13, no. 1, pp. 111–124, Jan./Feb. 2007.
[44] V. Vujicic *et al.*, "Mitigation of relative intensity noise of quantum dash mode-locked lasers for PAM4 based optical interconnects using encoding techniques," *Opt. Express*, vo. vol. 25, no. 1, pp. 20–29, 2017.
[45] K. Zhong *et al.*, "140-Gb/s 20-km transmission of PAM-4 signal at 1.3 μm for short reach communications," *IEEE Photon. Technol. Lett.*, vol. 27, no. 16, pp. 1757–1760, Aug. 2015.
[46] M. J. Heck *et al.*, "Analysis of hybrid mode-locking of two-section quantum dot lasers operating at 1.5 μm," *Opt. Express*, vol. 17, no. 20, pp. 18063–18075, 2009.

Zhenguo Lu received the Ph.D. degree in 1992. He is a Principal Research Officer, Team Lead of Photonics, and Project Leader with National Challenge Program "HTSN" with the Advanced Electronics and Photonics Research Centre of National Research Council (NRC), Ottawa, Canada. Since 2006, he is an Adjunct Professor with the Department of Electrical & Computer Engineering with both University of Ottawa and Concordia University, in Canada. He was the recipient of the Alexander von Humboldt (AvH) Research Fellowship to work with the Institute of Semiconductor Electronics, RWTH Aachen, Germany from 1993 to 1995. Then he worked at the Terahertz Research Centre of Rensselaer Polytechnic Institute, NY, USA for two years. He came to NRC as a Research Officer in 1997. From 2000 to 2002, he was the Director of the R & D, BTI Systems Inc., Ottawa. He re-joined NRC as a Senior Research Officer in 2002. He has authored or coauthored more than 250 journals and conference papers, and has eight US patents. He is an expert in the field of photonics devices and optical network system applications.

Jiaren Liu was born in Sichuan, China, in 1963. He received the B.S. and M.S. degrees in physics from the University of Sichuan, Chengdu, China, in 1983 and 1989, respectively, and the Ph.D. degree in optics from the Nanjing University of Science and Technology, Nanjing, China, in 1992. He was a Teaching Assistant at the Department of Physics, University of Sichuan from 1983 to 1987, an Associate Research Scientist at the Shanghai Institute of Optics and Fine Mechanics, Shanghai, China, from 1992 to 1996, a Postdoctoral Research Associate at Texas A&M University, USA and University of Toronto, Canada from 1996 to 1999, and a Product Design Engineer and Manager from 1999 to 2001. Since 2001, he has been a Senior Research Officer with National Research Council Canada. He is the author of more than 150 peer reviewed articles and several patents. His research interest includes quantum dot semiconductor lasers, fiber lasers, femtosecond laser micromachining, photonic devices, laser spectroscopy, quantum optics, and information optics.

Philip J. Poole received the B.Sc. degree in physics and the Ph.D. degree in solid state physics from Imperial College, University of London, in 1989 and 1993, respectively. Since 1993, he has worked with the National Research Council Canada (NRCC) in the areas of semiconductor optics and crystal growth. He is currently the Team Leader with the Epitaxy Team in the Advanced Electronics and Photonics Research Centre with the NRCC. His work has covered many areas of III-V semiconductor research including optical spectroscopy, quantum well intermixing, and 22 years of experience in CBE growth of III-V compounds. His research interests include the areas of epitaxial growth of InP-based quantum dot structures for optoelectronic devices that can take advantage of the novel properties of quantum dots, such as multiwavelength and femtosecond modelocked lasers. The use of selective area epitaxy to control the nucleation site of individual quantum dots for quantum information purposes is also studied. In particular the growth of InP nanowires containing InAs dots with the demonstration of non-classical optical properties such as photon antibunching and entanglement.

Youxin Mao received the B.S. and M.S. degrees in physics and electronics science from Nankai University, China, in 1982 and 1985, respectively, and the Ph.D. degree in opto-electronics from Lancaster University, U.K., in 1995. From 1995 to 1997, she was a Research Associate with the Lancaster University and from 1997 to 1999, she was a NSERC Visiting Fellowship at National Research Council in Canada. As a Research Scientist, she worked in Exploratory R&D group with JDS Uniphase from1999 to 2003 and in Medical Biophysics with the University of Toronto from 2003 to 2006. Since 2006, she has been a Senior Research Officer with National Research Council Canada. She is the author or coauthore of more than 130 peer reviewed articles. Her research interests include quantum dot semiconductor mode-locked laser, QAM data format coherent optical network, high speed and high power wavelength swept laser, semiconductor laser package, fiber optics, ultra-small optical fiber probe, and optical coherence tomography.

John Weber received the Bachelors of Mechanical Engineering degree from Carleton University in 1991. He had previously been with JDS Uniphase (now Lumentum), Nortel Networks and Scintrex Trace, in the development of a variety of electronic and fiber-optic components, test instrumentation, and sub-systems before joining the National Research Council in 2009. As part of the Advanced Electronics and Photonics team, he works with researchers to develop experimental and prototype package designs for novel electronic and photonic devices.

Guocheng Liu received the Ph.D. degree in electrical and computer engineering from the University of Waterloo, Canada, in 2015. From 2016 to 2017, he was a Postdoctoral Fellow at the University of Waterloo. From 2017 to 2019, he worked as an Optical Device Scientist at VueReal Inc. Since 2019, he has been a Research Associate with National Research Council Canada. His research interests include quantum dot semiconductor laser, ultrahigh-speed PAM, and QAM coherent optical networks.

Pedro Barrios received the B.Sc. degree in electronic engineering from the IUPFAN, Venezuela, in 1989, and the M.S. and Ph.D. degrees in electrical engineering from the University of Pittsburgh, Pittsburgh, USA, in 1993 and 1997, respectively. He worked as a Postdoc at the NanoFAB Center of Texas A&M University during 1998–1999 and at the Electrical Engineering Department of the University of Notre Dame from 1999 to 2000. He currently works with the Advanced Technology Fabrication group of the Advanced Electronics and Photonics Research Centre of the National Research Council of Canada, Ottawa, ON, Canada. He is currently working toward the research in fabrication of electronic and optoelectronic devices on Si and III-Vs semiconductors. He has also investigated the oxidation of III-V native oxides (AIGaAs and InAlP) with focus on materials, fabrication, and characterization of MOS and HEMT devices, as well as underwent research in electronic materials characterization and development of thin films and nanostructure devices on Si.